

RESEARCH

Open Access



Deep learning-based algorithm for classifying high-resolution computed tomography features in coal workers' pneumoconiosis

Hantian Dong^{1,2}, Biaokai Zhu³, Xiaomei Kong², Xuesen Su⁴, Ting Liu⁴ and Xinri Zhang^{2,4*}

*Correspondence:
XinriZhang@outlook.com

¹ First Department of Geriatric Diseases, First Hospital of Shanxi Medical University, No. 85 Jiefang South Road, Taiyuan 030001, Shanxi, People's Republic of China

² Department of Pulmonary and Critical Care Medicine, National Health Commission Key Laboratory of Pneumoconiosis, Shanxi Key Laboratory of Respiratory Diseases, First Hospital of Shanxi Medical University, No. 85 Jiefang South Road, Taiyuan 030001, Shanxi, People's Republic of China

³ Network Security Department, Shanxi Police College, Qingxu Country, No. 799 Qingdong Road, Taiyuan 030021, Shanxi, People's Republic of China

⁴ The First College for Clinical Medicine, Shanxi Medical University, No. 56 Xinjian South Road, Taiyuan 030001, Shanxi, People's Republic of China

Abstract

Background: Coal workers' pneumoconiosis is a chronic occupational lung disease with considerable pulmonary complications, including irreversible lung diseases that are too complex to accurately identify via chest X-rays. The classification of clinical imaging features from high-resolution computed tomography might become a powerful clinical tool for diagnosing pneumoconiosis in the future.

Methods: All chest high-resolution computed tomography (HRCT) medical images presented in this work were obtained from 217 coal workers' pneumoconiosis (CWP) patients and dust-exposed workers. We segmented regions of interest according to the diagnostic results, which were evaluated by radiologists. These regions were then classified regions into four categories. We employed an efficient deep learning model and various image augmentation techniques (DenseNet-ECA). The classification performance of the different deep learning models was assessed, and receiver operating characteristic (ROC) curves and accuracy (ACC) were used to determine the optimal algorithm for classifying CWP clinical imaging features obtained from HRCT images.

Results: Four primary clinical imaging features in HRCT images, with a total of more than 1700 regions of interest (ROIs), were annotated, augmented, and used as a training set for tenfold cross-validation to generate the model. We selected DenseNet-Attention Net as the optimal model through assessing the performance of different classification algorithms, which yielded an average area under the ROC curve (AUC) of 0.98, and all clinical imaging features were classified with an AUC greater than 0.92. For the individual classifications, the AUCs were as follows: small miliary opacities, 0.99; nodular opacities, 1.0; interstitial changes, 0.92; and emphysema, 1.0.

Conclusion: We successfully applied a data augmentation strategy to develop a deep learning model by combining DenseNet with ECA-Net. We used our novel model to automatically classify CWP clinical imaging features from 2D HRCT images. This successful application of a deep learning-data augmentation algorithm can help clinical radiologists by providing reliable diagnostic information for classification.

Trial registration: Chinese Clinical Trial Registry, ChiCTR2100050379. Registered on 27 August 2021, <https://www.chictr.org.cn/bin/project/edit?pid=132619>.



Keywords: Coal workers' pneumoconiosis classification, High-resolution computed tomography, Deep learning, DenseNet, ECA-Net, Data augmentation

Introduction

Coal workers' pneumoconiosis (CWP) is a chronic occupational lung disease associated with long-term inhalation of coal dust particles in the workplace. The main pathological feature of CWP is diffuse interstitial lung fibrosis [1]. Despite the substantial decline in the prevalence of CWP worldwide over the past several decades [2–4], recent findings have shown that the incidence of CWP has increased in the eastern United States and in Queensland, Australia. CWP is one of the most prevalently diagnosed types of pneumoconiosis across all age groups on the basis of the China National Report on Occupational Diseases, predominantly among males [5]. In addition, the overall prevalence of CWP is high, with the disease representing more than 6% of all occupational diseases in China alone. In 2016, for example, the number of newly confirmed cases of diagnosed pneumoconiosis exceeded 27,000 (website available: <http://www.nhfpc.gov.cn/>), more than 50% of which (16,658) were CWP (16 658) [6]. No specific therapy effectively delaying the disease progression of fibrosis and addressing the pulmonary complications of pneumoconiosis has been developed. Hence, improving the early diagnosis rates of CWP is important [7].

According to International Labour Organization (ILO) guidelines, chest X-rays are essential for early screening, staging, and diagnosis of pneumoconiosis. These latter two, however, can be complex and time-consuming processes, as the final diagnosis should be determined by expert panels, which often include well-trained and experienced occupational physicians and radiologists. Diagnoses are made according to the ILO guidelines and involve visually identifying subtle imaging features and combining them with factors such as exposure history and dust density for analysis. Although chest X-rays are the so-called gold standard for diagnosing pneumoconiosis, they do not provide sufficient details about opaque regions in the lungs; thus, unambiguous differential diagnoses between CWP and other types of pneumoconiosis are difficult to obtain [2, 8].

In contrast to primary prevention techniques and to enhance clinical prevention approaches, our understanding of the disease according to CWP clinical imaging features must be improved. Patients with CWP and dust-exposed workers may experience nonspecific symptoms such as cough, chest tightness, shortness of breath, and dyspnoea upon exertion, with infiltrates usually noted on lung images. Under these circumstances, clinical doctors in general hospitals are often the best resource for providing comprehensive assessments according to the patient's condition and determining clinical imaging features for further evaluation, diagnosis, and treatment.

However, owing to overlapping pneumoconiosis infiltration, radiological approaches generally perform poorly in diagnosing pulmonary complications of pneumoconiosis [9]. High-resolution computed tomography (HRCT) can be applied to address limitations in the differential diagnosis of CWP-related pulmonary complications, as HRCT scans may be more sensitive and specific than chest X-rays are [10]. However, HRCT has not yet been accepted for general screening, staging, and diagnosis of various types of

pneumoconiosis because of the absence of a unified global standard [2, 11]. Therefore, our knowledge of the CWP imaging features on HRCT images must be improved.

In recent years, the results of several studies have demonstrated that medical images can be classified via artificial intelligence (AI) and deep learning (DL) algorithms [12–17], which have achieved performances comparable to those of medical imaging experts to a certain extent. DL is a branch of AI that has shown remarkable success in medical image analysis, especially in detecting pneumoconiosis [18–23]. In our previous study, we used a DL technique and a data augmentation model [19] and successfully built a computer-aided classification system (constructed by combining ShuffleNet V2 with ECA-Net) to classify CWP clinical imaging features from chest radiographs, thus providing more references for clinical application.

In this paper, we propose a deep learning classification algorithm and data augmentation technique based on our previous study that obtains sufficient image details, thereby revealing the uniqueness of CWP clinical imaging features obtained by analysing HRCT image data.

Results

Distribution of HRCT clinical imaging features

The lesions were categorized into four main types according to their HRCT imaging features. The specific distribution range of all lesions analysed in this study was obtained and recorded in detail. Table 1 summarizes the detailed distribution of the clinical chest HRCT imaging features. The lesions were categorized into four main types according to their HRCT imaging features.

Classification results of different models

Figure 1 illustrates the study flow. To classify the CWP features in HRCT images, we evaluated the performance of different models and selected the optimal model through comparisons and analyses. The experimental results are shown in Table 2.

Accuracy

Figure 2 shows that the DenseNet-Attention algorithm achieves the best accuracy among the five models. The average accuracies of the models using DenseNet-Attention as the

Table 1 Distribution of HRCT clinical imaging features

Location of lung zones	HRCT features (number of ROIs)			
	Pulmonary nodules–small military opacities	Pulmonary nodules–nodular opacities	Pulmonary interstitial changes	Emphysema
Top-right	239	19	5	53
Middle-right	198	113	40	21
Bottom-right	89	53	45	29
Top-left	247	12	3	43
Middle-left	164	98	63	22
Bottom-left	63	45	57	33
Total	1000	340	213	201

ROIs regions of interest

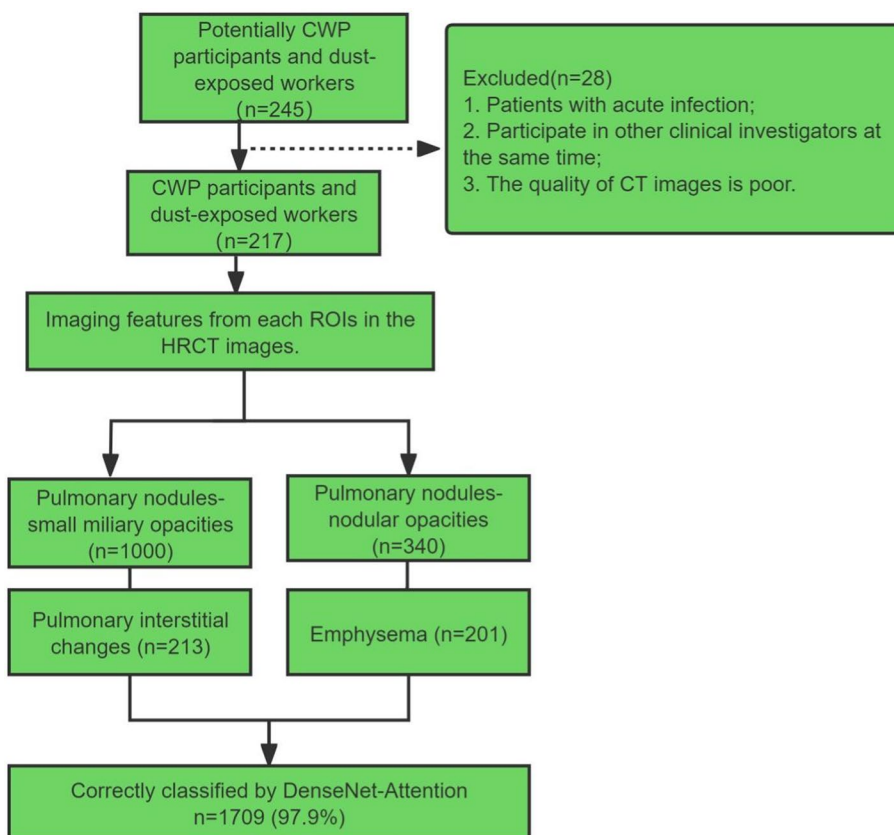


Fig. 1 Flowchart of the diagnostic accuracy study

Table 2 Evaluation results of DenseNet-Attention and other DL algorithms

	Accuracy	Recall	F1-score	Weighted avg	Precision			
					A	B	C	D
DenseNet-Attention	0.96	0.97	0.95	0.97	0.99	0.99	0.86	0.99
DenseNet121	0.94	0.95	0.94	0.94	0.96	0.97	0.85	0.98
ResNet-50	0.91	0.92	0.92	0.91	0.91	0.89	0.81	0.9
MobileNet	0.88	0.89	0.88	0.89	0.92	0.93	0.83	0.84
Shufflenet v2	0.85	0.89	0.87	0.9	0.91	0.82	0.77	0.85

Class A: pulmonary nodules–small miliary opacities, Class B: pulmonary nodules–nodular opacities, Class C: pulmonary interstitial changes, Class D: emphysema

backbone were significantly higher than those of the other models. With sufficient training, the accuracy of DenseNet-Attention was slightly higher than that of DenseNet121 after 10 epochs. DenseNet-Attention obtained the highest accuracy (>95%) after the 30th epoch, demonstrating the promising performance of our proposed algorithm in classifying CWP features in HRCT images.

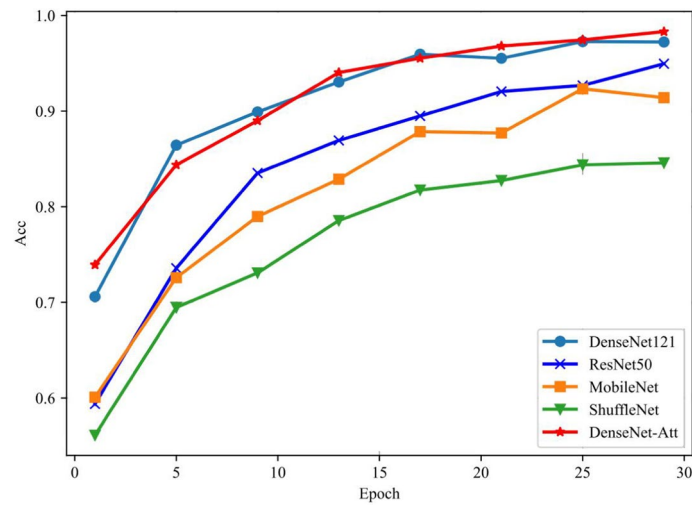


Fig. 2 Classification accuracy of different models as a function of the number of epochs

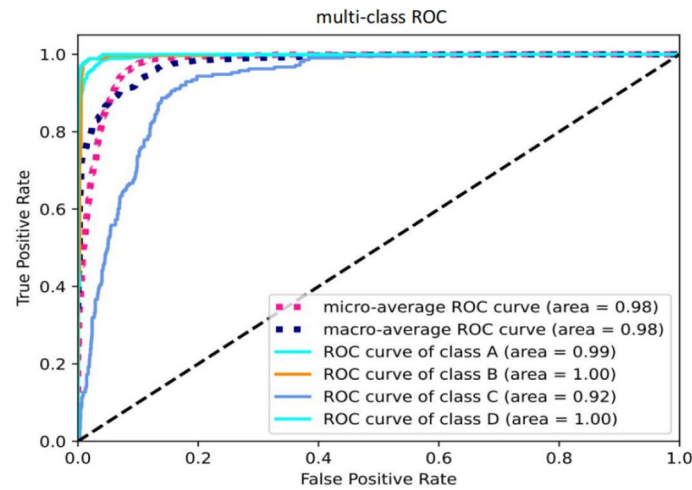


Fig. 3 ROC curves of the model in classifying different categories. Class A: pulmonary nodules–small miliary opacities, Class B: pulmonary nodules–nodular opacities, Class C: pulmonary interstitial changes, Class D: emphysema

ROC curve analysis

The ROC curves were analysed to evaluate the image feature classification ability of the different models, as shown in Fig. 3. On the basis of the accuracy results, we selected the DenseNet-Attention model for further analysis, as it achieved the best performance among the compared models. We compared the different classification models in terms of the AUC. The average AUC of the overall classification was 0.98; for the individual classifications, the AUCs were as follows: small miliary opacities (Class A), 0.99; nodular opacities (Class B), 1.0; interstitial changes (Class C), 0.92; and emphysema (Class D), 1.0.

Discussion

Imaging examination is crucial for the diagnosis and treatment of occupational pneumoconiosis. Presently, the process of diagnosing occupational pneumoconiosis relies heavily on comparing patients' chest X-ray images to a standardized reference film, and the early detection rate of CWP is relatively low. In addition, patients with early CWP have lung function damage, and there are no obvious clinical symptoms. With the progression of the disease, these patients may present with symptoms such as chest tightness, dyspnoea and haemoptysis, which occur in a variety of primary or secondary diseases, such as pulmonary tuberculosis and lung cancer.

According to our identified HRCT imaging feature classification performed in this study, different clinical imaging features may be more indicative of underlying diseases in terms of secondary prevention. Differentiating pulmonary nodules—small miliary opacities and pulmonary nodules—nodular opacities on the basis of nodule size (lesions greater or less than 5 mm in size) might be beneficial for the clinical differential diagnosis of pulmonary complications of CWP, such as pulmonary tuberculosis and the early stages of lung cancer. Similarly, assessing the features of pulmonary interstitial changes and emphysema might be advantageous for the early identification of interstitial lung disease or pneumothorax. Early clinical diagnosis of CWP may lead to early corresponding treatment measures, thus controlling symptoms, improving quality of life, reducing the incidence of hospitalization, and improving quality of life and survival prospects for CWP patients.

In recent years, an increasing number of researchers have focused on active screening and staging for pneumoconiosis using chest clinical imaging. Zhang et al. [18] developed a deep learning-based model for screening and staging pneumoconiosis, whose accuracy was 0.973, with both sensitivity and specificity greater than 0.97. Sun et al. [22] proposed a fully deep learning paradigm for pneumoconiosis staging on chest radiographs, with an accuracy of 90.4% and an AUC of 96%. In 2024, Liu et al. [23] used the multistage joint approach of Res-Net 34 in combination with image enhancement and the U-Net model for image segmentation and achieved an accuracy of 89%, with an AUC of 0.98 and a high QWK score of 0.94. Another 2024 study revealed that a self-developed TM-Net neural network (ResNet neural network) helped screen for pneumoconiosis in chest radiographs with high performance (its accuracy was 95%, its AUC was 94.7%, and its sensitivity was 100%) on the basis of 49,872 chest radiographs. However, in contrast to the above studies, our study focused specifically on CWP and aimed to construct a clinically reliable classification model based on the clinical imaging features of CWP by considering potential deep learning algorithms and well-annotated HRCT image data. It is generally known that screening and staging pneumoconiosis from chest radiographs for differential diagnosis, early evaluation and early treatment of CWP are less effective than analysing lesion areas on HRCT images in clinical settings. In addition, high-resolution computed tomography (HRCT) has been identified as irreplaceable in the differential diagnosis of pulmonary complications of CWP. Therefore, it is reasonable and meaningful to attempt to systematically analyse the clinical imaging features of CWP in HRCT data and to use well-established deep learning techniques and data augmentation models.

However, our study has several limitations. First, there is still a lack of clear and unified criteria for the diagnosis of CWP in chest HRCT images. In this study, the standards for the diagnosis and classification of CWP with chest HRCT images relied primarily on clinical imaging diagnostic reports confirmed by experienced clinicians that fulfilled disease-specific diagnostic criteria. Second, as in related deep learning-based applications, the most common limitation of image feature classification is the sample size. When more experimental data are available, more useful feature information can be obtained to refine the deep learning model. Since the research design was exploratory, a power analysis was not conducted to determine the study's sample size. As shown in our study and previous works [2, 10, 11, 19], CWP lacks HRCT imaging diagnostic criteria but has similar imaging features in different stages of pneumoconiosis. We obtained 217 patient samples from a cohort study, which may not be sufficient to obtain a meaningful conclusion. Despite this limitation, the present research adequately discerned the correct classification results among these groups. Finally, this research focused on classifying four types of CWP clinical imaging features; however, as seen from the clinical HRCT images of CWP patients, none of these specific lung areas represented a typical disease pattern. Moreover, determining the specific source of clinical imaging features (opacities, interstitial changes, or emphysema) from different diseases, such as primary CWP, secondary tuberculosis, or other lung disorders or infections, remains complicated.

Thus, relying solely on diagnostic imaging methods may result in inaccurate clinical diagnoses, and combining clinical examinations and serological tests may provide additional evidence to comprehensively characterize CWP patients. Therefore, this topic merits further attention and exploration.

Conclusion

We successfully applied a data augmentation strategy to develop a deep learning model by combining DenseNet with ECA-Net and used our novel approach to automatically classify CWP clinical imaging features from 2D HRCT images. Among the studied models, DenseNet-Attention was determined to be the best, achieving an average accuracy of 98% on the imaging dataset. Moreover, the combination of multiple models was more beneficial for clinical imaging classification. We applied the DL-based model in a clinical environment and analysed chest HRCT imaging data to enhance our understanding of the imaging characteristics of pneumoconiosis-related lung diseases, which may improve the utilization of HRCT imaging to establish diagnostic criteria for pneumoconiosis in the future.

Materials and methods

Study design

This study followed the STARD 2015 guidelines, and it was a prospective, single-centre study.

Data collection

In this study, all participants voluntarily participated in a CWP-based prospective cohort study that enrolled individuals with CWP and dust-exposed workers with symptoms

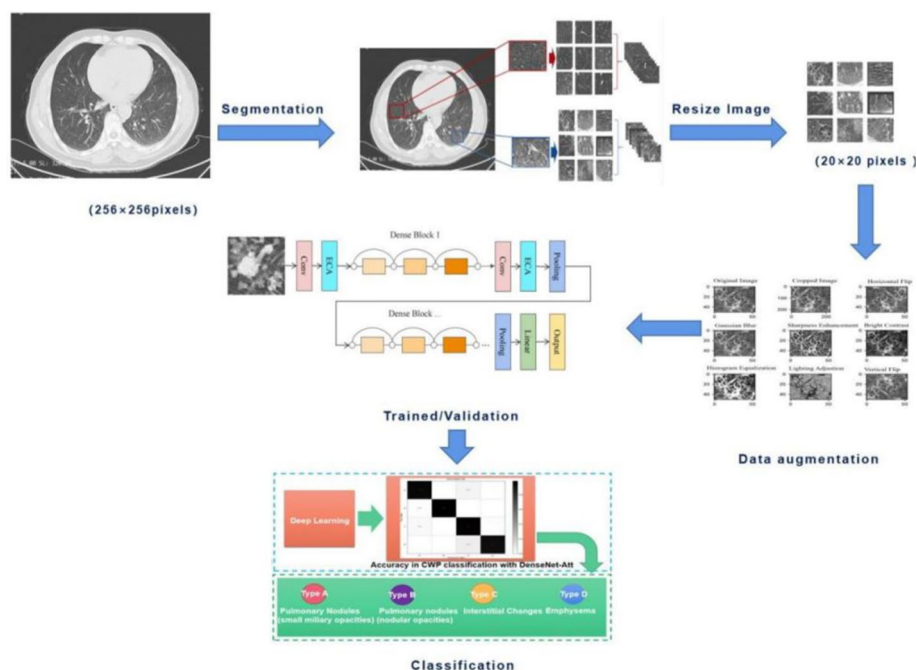


Fig. 4 Overview of the proposed DL model training and evaluation method

such as cough, dyspnoea, and fatigue from coal mines near Taiyuan city. Before participant recruitment, all necessary approvals from the regulatory and provincial health departments were obtained, and all participants of the study were randomly selected according to lists provided by the Municipal Center for Disease Control and Prevention of Taiyuan city. The participants completed the baseline survey and first clinical examination between 28 August 2021 and 12 December 2023. The inclusion criteria were as follows: (1) coal mining workers with more than 15 years of working experience (with a clear history of dust exposure), male, and aged 35 to 80 years; (2) clinical symptoms such as cough and shortness of breath; (3) complete clinical data (perfect blood routine, liver and kidney function, blood sugar, blood lipids, blood pressure, ESR, procalcitonin, etc.); (4) clinical diagnosis of pneumoconiosis that met the diagnostic criteria; and (5) voluntary participation in this study and signed informed consent. Participants with any of the following conditions were excluded: (1) acute infection, (2) participation by other clinical investigators at the same time, or (3) poor-quality CT images. As this was an exploratory study, no sample size was calculated. A schematic diagram describing the primary processing steps for the proposed method is depicted in Fig. 4. During this baseline period, all patients were asked to complete a routine clinical examination, including laboratory examinations, chest radiography and chest HRCT. In total, we used the chest HRCT images of 217 patients with CWP for analysis.

Baseline demographic and clinical characteristics of the participants

Among the participants, we selected male patients with an apparent history of occupational exposure to coal dust (more than 15 years, with an average exposure of 29.8 ± 13.9 years) between the ages of 35–80 years for inclusion in the study. None of our participants experienced any complications from the study, or any side effects occurred

Table 3 Baseline participant characteristics

	All subjects	Dust-exposed workers	CWP Stage I M (SD)	CWP Stage II	CWP Stage III	
Age (yr), mean (SD)	54.7 (12)	48.9 (6.1)	60.2 (10.3)	58.3 (8.3)	57.1 (7.3)	
Exposure duration (yr), mean (SD)	29.8 (13.9)	22.1 (8.2)	31.6 (9.5)	26.6(12.8)	18.1 (2.2)	
Dyspnoea (SD)	3 (8)	0 (3)	5 (7)	5 (9)	3.7 (2.1)	
Cough (SD)	0.5 (5)	0 (3)	3 (7)	0 (6)	8.9 (5.2)	
mMRC score (SD)	3 (3)	0 (2)	3 (3)	2 (0)	1.6 (0.9)	
Number						
Industry type		217	60	129	25	3
	Mining (n)	60	30	26	4	0
	Tunnelling (n)	99	27	56	14	2
	Mixing (n)	22	0	18	3	1
	Comprehensive digging (n)	21	1	17	3	0
	Other (n)	15	2	12	1	0

M mean, SD standard deviation, mMRC modified Medical Research Council

during the HRCT scan. The main clinical characteristics and industry types of the participants by CWP stage are reported in Table 3.

Scanner specifications

All the HRCT image data used in this study, which were acquired using the Digital Imaging and Communications in Medicine (DICOM) standard (version 3.0), were collected with a third-generation Siemens dual-source CT device (Somatom Definition, Siemens, Germany) or a Philips IQon 128-slice spectral CT (Philips Healthcare, Cleveland, OH, USA). The acquisition parameters were as follows. Spectral CT images were obtained with a circular orbit with a 360° arc, 128×128 matrix, zoom 1, 140 keV photopeak, and 90 images of eight seconds per image. The acquired CTs used 120 kV, 50–350 mA, with a slice thickness and interval of 1.25 mm (General Electric) and 3 mm (Siemens). The HRCT parameters were as follows: tube voltage of 120 kV, tube current of 150–350 mA, section thickness of 5 mm, reconstruction interval of 5 mm, lung window width/level of 500–1100 HU, mediastinal window of 350–40 HU, detector collimation of 64–0.625 mm, and rotation time of 0.75 s.

Feature classification and selection

High-quality image feature extraction is a prerequisite of image feature analysis and is currently the best available method for simplifying high-dimensional image data [17]. To identify clinical diagnosis-specific features of CWP in HRCT images, during the diagnosis period, initial reports were obtained from four radiologists with 5–10 years of experience and reviewed independently by two senior radiologists with more than 10 years of experience who agreed upon the final diagnosis. Given the descriptive and mechanistic

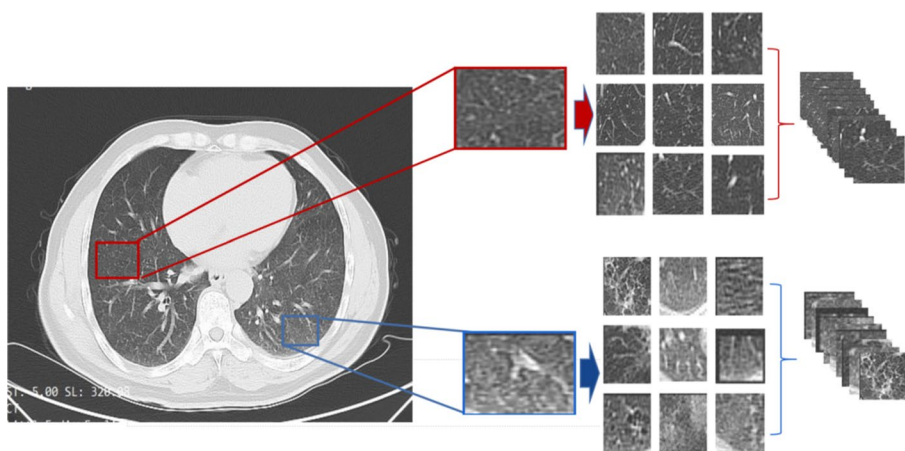


Fig. 5 Preprocessing of original image data: slices chosen for region of interest (ROI) delineation

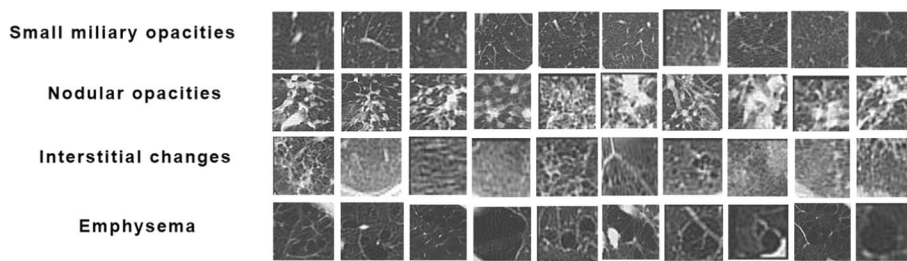


Fig. 6 Examples of ROIs used for CWP clinical HRCT imaging feature-based classification

nature of HRCT imaging features, this trial was designed as an exploratory study without prespecified effects.

As reported in previous studies [24–27], the respiratory complications of CWP mainly include pulmonary tuberculosis, pneumothorax, interstitial lung disease, and lung cancer. For comparison, previous studies on CWP have focused mainly on the diagnosis and stages of pneumoconiosis in chest X-rays. In our study, according to the abovementioned chest HRCT diagnosis reports, different clinical imaging features may be more indicative of underlying diseases in terms of secondary prevention. In these reports, four primary clinical imaging features of CWP were classified in the HRCT images: (A) pulmonary nodules–small miliary opacities, (B) pulmonary nodules–nodular opacities, (C) pulmonary interstitial changes, and (D) emphysema.

Referring to some previous studies, we extracted features from each region of interest (ROI) using handcrafted rules [28–30] according to the diagnosis reports. Moreover, these images were segmented according to the 20 × 20 pixels ROIs in the HRCT images and saved as JPEG images for analysis. This process is presented in Fig. 5.

The ROIs were assigned the following data labels, as illustrated in Fig. 6: pulmonary nodules–small miliary opacities ($n = 1000$), pulmonary nodules–nodular opacities ($n = 340$), pulmonary interstitial changes ($n = 213$), and emphysema ($n = 201$). These ROIs were used as a training set to generate the model.

Feature preprocessing and data augmentation in image classification

Many related studies have shown that data augmentation is crucial for improving the accuracy of classification algorithms [18, 31–34]. In our previous study, image data augmentation was successfully employed to analyse the clinical imaging features of CWP in chest X-ray images. All the images were scaled to the same size (100×100 pixels) to ensure that they could be easily input into the model. Considering the specificities of CT image data, we adopted various augmentation methods for classification, such as random rotation, sharpness enhancement, random horizontal flipping, Gaussian blurring, image histogram equalization, and random brightness alteration. Table 4 presents the samples used in the chest HRCT data augmentation process.

Implementation details

First, we performed conventional data augmentation (basic image manipulation) on the ROIs, which yielded more than 7000 training data points. All data points were used for the analyses, and there were no missing values for the imaging data. Tenfold cross-validation was applied to randomly divide the original dataset into a training set (70% of the data), a validation set (20% of the data), and a test set (10% of the data). In the ten rounds of training, nine groups were used for training, and the remaining group was adopted as the test data; thus, 16 images were trained during each round. Furthermore, the number of training epochs was set to 30, the initial learning rate was set to 0.0001, and four categories were considered in the classification task. All the models in this research were implemented in PyTorch version 1.7.0, and the codes were run on a server with an RTX 2080Ti GPU.

DenseNet with ECA-attention net (DenseNet-attention)

DenseNet

The densely connected convolutional network (DenseNet), which is different from traditional CNN architectures, is composed of two structures (dense blocks and transition layers), thus introducing direct connections between any two layers using imaging features of the same size [35]. The original DenseNet consists of densely connected convolutional networks between dense blocks. Moreover, DenseNet adopts a mechanism in which all input connections can process the imaging features and are interconnected with layers at all resolution levels, with the output of one layer serving as the input for the next layer.

In our study, all the layers in DenseNet are connected [36]. This approach is known for its advantages in the gradient backpropagation method, including decreasing the training time, reducing the number of parameters and computations in the model and significantly accelerating the training speed, thus effectively using powerful low-level features owing to feature reuse.

Efficient channel attention network (ECA-Net)

The channel attention mechanism has been shown to improve the accuracy of CNN models. In 2020, Wang et al. [37] proposed an efficient channel attention (ECA) module as a “plug-and-play”, lightweight attention module that generates channel

Table 4 Detailed classification after image dataset augmentation

Classification	Image data augmentation examples				
Interstitial changes	Original Image	Cropped Image	Horizontal Flip		
	Gaussian Blur	Sharpness Enhancement	Bright Contrast		
	Histogram Equalization	Lighting Adjustment	Vertical Flip		
	Nodular opacities	Original Image	Cropped Image	Horizontal Flip	
		Gaussian Blur	Sharpness Enhancement	Bright Contrast	
		Histogram Equalization	Lighting Adjustment	Vertical Flip	
		Emphysema	Original Image	Cropped Image	Horizontal Flip
			Gaussian Blur	Sharpness Enhancement	Bright Contrast
			Histogram Equalization	Lighting Adjustment	Vertical Flip

attention by using fast 1D convolution to ensure model efficiency and accuracy. It requires only a small number of parameters to produce apparent performance improvements. ECA-Net can also lead to significant model accuracy improvements despite the use of finite sample data, thus improving the ability to classify imaging features.

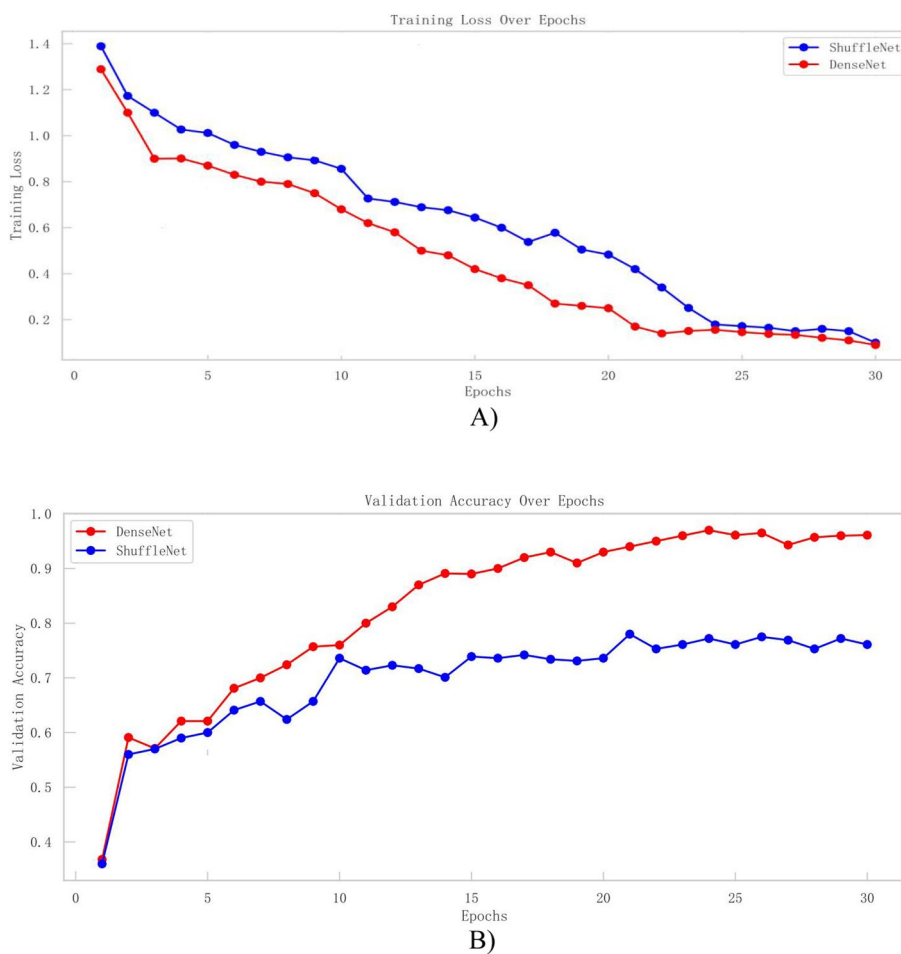


Fig. 7 Comparative analysis of the attention mechanism. **A** Training losses between different attention mechanisms with epochs. **B** Validation accuracy between different attention mechanisms with epochs

DenseNet-attention

According to the results of the preexperiment, when the original DenseNet121 was used for classification training, pulmonary interstitial changes and pulmonary nodule–small miliary opacities were occasionally confused. Thus, we implemented ECA [37, 38] to improve model accuracy, thus increasing the ability to classify imaging features.

The main field application of computer vision consists of medical imaging analysis in CNNs, which has high requirements for channel and spatial attention. Among the different kinds of attention mechanisms, ShuffleNet-Attention and DenseNet-Attention achieve outstanding performance in this regard. This work employed a classification model, AlexNet, which was applied to ShuffleNet-Attention and DenseNet-Attention. The comparative analysis between the attention mechanism, by plotting their loss curves and accuracy curves, allowed us to choose the one that performed better to fulfil this research need. As the results of Fig. 7 show, all the simulations were run for the same number of epochs, higher validation accuracy and lower training loss were achieved in DenseNet-Attention. In addition, in view of the large amount of data contained in HRCT clinical imaging, the ShuffleNet-ECA attention model was more suitable for the analysis

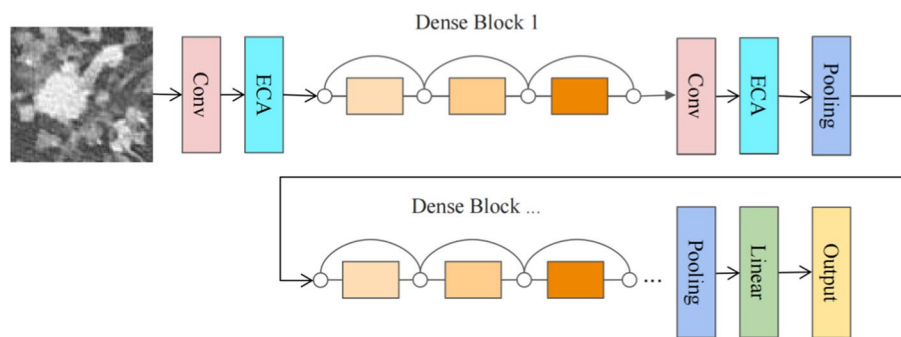


Fig. 8 Model construction for improving performance: integrating DenseNet with ECA-Net

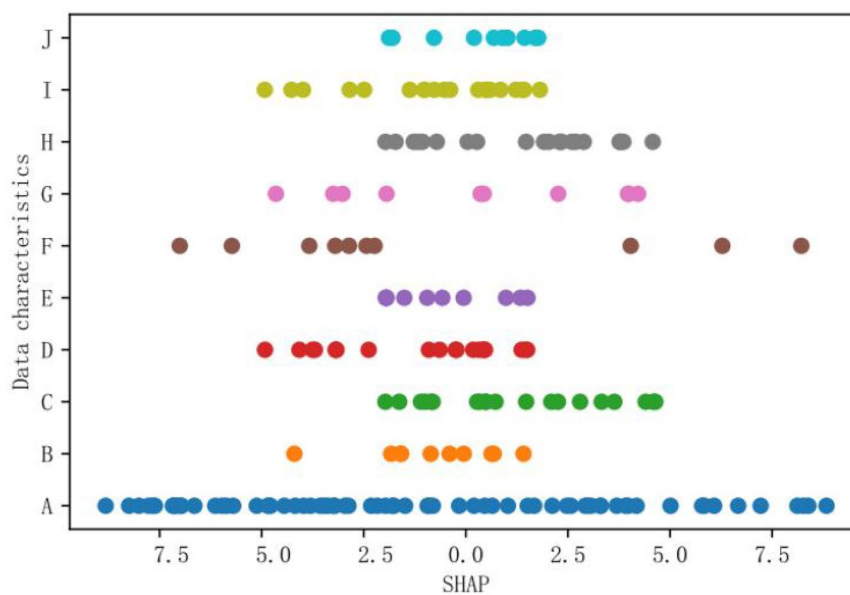
of lightweight datasets, so the analysis effect on HRCT datasets using ShuffleNet-ECA attention was suboptimal, which required significantly more features and running time. Therefore, we chose DenseNet-Attention as the network of interest in this study.

To prevent the above feature misidentification, DenseNet is used as the backbone of the model for processing sensory inputs. Beginning with the first DenseNet block, the convolutional layers in each DenseNet block are assigned to the corresponding ECA-Net block, with a self-adaptive kernel size used for the 1D and local convolutions across channels without applying dimensionality reduction. This approach improves the performance with only a small number of simple parameters. Figure 8 depicts the process of combining DenseNet with ECA-Net and uses a mathematical formula to describe DenseNet and ECA attention in the supplementary material.

Application of explainable artificial intelligence (XAI) in this deep learning-based classification algorithm

In the interdisciplinary field of artificial intelligence and medicine, many researchers have recognized that successful AI deployment in clinical environments should not rely solely on model accuracy but also prioritize model explainability [39]. In this study, we applied SHAP (SHapley Additive exPlanations), a model explanation package developed in Python. By creating SHAP summary plots to visualize the model features and to provide an intuitive understanding of the overall pattern, the main principle of the study design is to draw a line chart on the model output on the basis of the value of each feature from each sample. We treated all the features as contributors, and the model produced a prediction value from each prediction sample. The SHAP value was assigned to each feature in each sample, which was sorted in alphabetic order (A–J), as displayed in Fig. 9.

The 10 clinical imaging features were confirmed on the basis of the diagnostic reports and XAI method; however, some features, such as pleural plaques and mediastinal masses, were not analysed in the DL model, as they were severely underrepresented on chest HRCT imaging ($n < 10$); the other imaging features (cord-like shadows, vascular calcifications, enlarged lymph nodes and pleural thickening) have no proven diagnostic value in HRCT imaging. From the figure, among the 10 imaging features, feature A, whose SHAP value distribution range ranged between $[-10, 10]$, clearly had the greatest influence on the outcome, showing a wide range distribution with high discriminant validity. The



Details of data characteristics:

- A) Pulmonary nodules-small miliary opacities
 - C) Pulmonary interstitial changes
 - E) Mediastinal masses
 - G) Cord-like shadow
 - I) Enlarged lymph nodes
- B) Pulmonary nodules-nodular opacities
 - D) Emphysema
 - F) Pleural plaques
 - H) Vascular calcifications
 - J) Pleural thickening

Fig. 9 HRCT imaging feature analysis using the explainable artificial intelligence (XAI) method

worst-performing feature was feature F, which was unevenly scattered and less numerous, leading to suboptimal output.

Model evaluation indicators

We employed two traditional performance measures in this study: accuracy and AUC. In addition, the algorithm performance was assessed through the following conventional metrics: precision, recall, and F1-score.

Here, accuracy is defined as the number of CWP clinical features that were correctly identified divided by the total number of classified CWP clinical features. The precision is calculated as the probability of making correct positive classifications, and the recall is calculated as the proportion of correct classifications. In addition, the F1-score, a metric that represents classification performance, is the harmonic mean of the precision and recall, which takes values in the interval [0, 1]. The higher the score is, the more correct the classification of CWP clinical features.

$$Accuracy = \frac{\text{Total of all True Classification}}{\text{Total of all images Classification}} \tag{1}$$

$$\text{Precision} = \frac{\text{Total of all True Positive classifications (TP)}}{\text{Total of all True Positive classifications (TP)} + \text{Total of all False Positive classifications (FP)}} \quad (2)$$

$$\text{Recall} = \frac{\text{Total of all True Positive classifications (TP)}}{\text{Total of all True Positive classifications (TP)} + \text{Total of all True Negative classifications (TN)}} \quad (3)$$

$$\text{F1-Score} = \frac{2 \times \text{Precision} \times \text{Recall}}{\text{Precision} + \text{Recall}} \quad (4)$$

To assess the ability of the DL model to correctly classify the CWP clinical features, the classification accuracy was evaluated according to the ROC curve and AUC.

Data analysis

The statistical analysis of baseline information was conducted using the software tool SPSS 23.0 (IBM, Armonk, NY). Age and mMRC were summarized using means and standard deviations and compared using independent Student's *t* test. According to the classification results of the radiologists, evaluation indicators such as accuracy, precision, recall, and F1-score were calculated using the deep learning algorithm. ROC curves and prediction results were generated using Python. Deviations of $p < 0.05$ were considered statistically significant.

Supplementary Information

The online version contains supplementary material available at <https://doi.org/10.1186/s12938-025-01333-4>.

Supplementary Material 1.

Acknowledgements

All the authors gratefully acknowledge the financial support from the National Health Commission Key Laboratory of Pneumoconiosis, Shanxi China Project and the Shanxi Province Key Laboratory of Respiratory Disease. We thank radiologist Dr. Qiao Ying and his group from the First Hospital of Shanxi Medical University for providing imaging diagnosis reports on all HRCT images at the First Hospital of Shanxi Medical University.

Author contributions

H.D. designed and conceived this research, participated in image data collection and interpretation of all data, and wrote this manuscript. B.Z. took full responsibility for the DL algorithm and statistical analysis. X.K. was responsible for supervision of the HRCT data collection and data management and was involved in reviewing this manuscript. X.S. and T.L. performed ROI data collection and data assembly. X.Z. supervised the data quality control and data analyses, interpreted the DL algorithm analyses, and critically reviewed the manuscript. All authors have read and consented to the final manuscript.

Funding

Organization: The National Health Commission Key Laboratory of Pneumoconiosis Shanxi China Project; Project number: 2020-PT320-005; Project Leader: Xinri Zhang; Department of Science and Technology of Shanxi Province; Project number: 202303021222345; Project Leader: Hantian Dong.

Availability of data and materials

Data are provided within the manuscript.

Declarations

Ethics approval and consent to participate

All the patients involved in the study provided written informed consent to participate. All CWP patients were diagnosed and confirmed according to the 2015 GBZ70-2015 Diagnostic Criteria for Pneumoconiosis. Ethical approval for the study (reference no. 2020K-K104) was given by the Research Ethics Committee of the First Hospital of Shanxi Medical University. All methods used in this manuscript were implemented in accordance with the relevant guidelines and regulations of the Declaration of Helsinki.

Consent for publication

All participants provided consent for data analysis and publication.

Consent for publication

Not applicable.

Informed consent

All the subjects provided written informed consent for participation in this study.

Competing interests

The authors declare no competing interests.

Received: 15 October 2024 Accepted: 6 January 2025

Published online: 27 January 2025

References

1. Wang T, Sun W, Wu H, Cheng Y, Li Y, Meng F, Ni C. Respiratory traits and coal workers' pneumoconiosis: Mendelian randomisation and association analysis. *Occup Environ Med.* 2021;78(2):137–41.
2. Qi XM, Luo Y, Song MY, Liu Y, Shu T, Liu Y, Pang JL, Wang J, Wang C. Pneumoconiosis: current status and future prospects. *Chin Med J (Engl).* 2021;134(8):898–907.
3. Xu G, Chen Y, Eksteen J, Xu J. Surfactant-aided coal dust suppression: a review of evaluation methods and influencing factors. *Sci Total Environ.* 2018;639:1060–76.
4. Blanc PD, Seaton A. Pneumoconiosis Redux. Coal workers' pneumoconiosis and silicosis are still a problem. *Am J Respir Crit Care Med.* 2016;193(6):603–5.
5. Zhao JQ, Li JG, Zhao CX. Prevalence of pneumoconiosis among young adults aged 24–44 years in a heavily industrialized province of China. *J Occup Health.* 2019;61(1):73–81.
6. Wang T, Li Y, Zhu M, Yao W, Wu H, Ji X, Hu Z, Shen H, Fan X, Ni C. Association analysis identifies new risk loci for coal workers' pneumoconiosis in Han Chinese Men. *Toxicol Sci.* 2018;163(1):206–13.
7. Dong H, Zhu B, Kong X, Zhang X. Efficient clinical data analysis for prediction of coal workers' pneumoconiosis using machine learning algorithms. *Clin Respir J.* 2023;17(7):684–93.
8. Perret JL, Plush B, Lachapelle P, Hinks TS, Walter C, Clarke P, Irving L, Brady P, Dharmage SC, Stewart A. Coal mine dust lung disease in the modern era. *Respirology.* 2017;22(4):662–70.
9. Jun JS, Jung JJ, Kim HR, Ahn MI, Han DH, Ko JM, Park SH, Lee HG, Arakawa H, Koo JW. Complications of pneumoconiosis: radiologic overview. *Eur J Radiol.* 2013;82(10):1819–30.
10. Wang X, Yu J, Zhu Q, Li S, Zhao Z, Yang B, Pu J. Potential of deep learning in assessing pneumoconiosis depicted on digital chest radiography. *Occup Environ Med.* 2020;77(9):597–602.
11. Şener MU, Şimşek C, Özkara Ş, Evran H, Bursalı İ, Gökçek A. Comparison of the International Classification of High-resolution Computed Tomography for occupational and environmental respiratory diseases with the International Labor Organization International Classification of Radiographs of Pneumoconiosis. *Ind Health.* 2019;57(4):495–502.
12. Devnath L, Fan Z, Luo S, Summons P, Wang D. Detection and visualisation of pneumoconiosis using an ensemble of multi-dimensional deep features learned from chest X-rays. *Int J Environ Res Public Health.* 2022;19(18):11193.
13. Devnath L, Luo S, Summons P, Wang D, Shaukat K, Hameed IA, Alrayes FS. Deep ensemble learning for the automatic detection of pneumoconiosis in coal worker's chest x-ray radiography. *J Clin Med.* 2022;11(18):5342.
14. Hao C, Jin N, Qiu C, Ba K, Wang X, Zhang H, Zhao Q, Huang B. Balanced convolutional neural networks for pneumoconiosis detection. *Int J Environ Res Public Health.* 2021;18(17):9091.
15. Barshooi AH, Amirkhani A. A novel data augmentation based on Gabor filter and convolutional deep learning for improving the classification of COVID-19 chest X-Ray images. *Biomed Signal Process Control.* 2022;72: 103326.
16. Singh R, Kalra MK, Nitiwarangkul C, Patti JA, Homayounieh F, Padole A, Rao P, Putha P, Muse VV, Sharma A, et al. Deep learning in chest radiography: detection of findings and presence of change. *PLoS ONE.* 2018;13(10): e0204155.
17. Li Z, Wu F, Hong F, Gai X, Cao W, Zhang Z, Yang T, Wang J, Gao S, Peng C. Computer-aided diagnosis of spinal tuberculosis from CT images based on deep learning with multimodal feature fusion. *Front Microbiol.* 2022;13:82334.
18. Zhang L, Rong R, Li Q, Yang DM, Yao B, Luo D, Zhang X, Zhu X, Luo J, Liu Y, et al. A deep learning-based model for screening and staging pneumoconiosis. *Sci Rep.* 2021;11(1):2201.
19. Dong H, Zhu B, Zhang X, Kong X. Use data augmentation for a deep learning classification model with chest X-ray clinical imaging featuring coal workers' pneumoconiosis. *BMC Pulm Med.* 2022;22(1):271.
20. Yang F, Tang ZR, Chen J, Tang M, Wang S, Qi W, Yao C, Yu Y, Guo Y, Yu Z. Pneumoconiosis computer aided diagnosis system based on X-rays and deep learning. *BMC Med Imaging.* 2021;21(1):189.
21. Litjens G, Kooi T, Ehteshami B, Arnaud B, Adiyoso A. A survey on deep learning in medical image analysis. *Med Image Anal.* 2017;42:60.
22. Sun W, Wu D, Luo Y, Liu L, Zhang H, Wu S, Zhang Y, Wang C, Zheng H, Shen J, et al. A fully deep learning paradigm for pneumoconiosis staging on chest radiographs. *IEEE J Biomed Health Inform.* 2022;26(10):5154–64.
23. Liu C, Fang Y, Xie Y, Zheng H, Li X, Wu D, Zhang T. Deep learning pneumoconiosis staging and diagnosis system based on multi-stage joint approach. *BMC Med Imaging.* 2024;24(1):165.
24. Koul A, Bawa RK, Kumar Y. Artificial intelligence techniques to predict the airway disorders illness: a systematic review. *Arch Comput Methods Eng.* 2022;30:1–34.
25. Jin Y, Fan JG, Pang J, Wen K, Zhang PY, Wang HQ, Li T. Risk of active pulmonary tuberculosis among patients with coal workers' pneumoconiosis: a case-control study in china. *Biomed Environ Sci.* 2018;31(6):448–53.
26. Leonard R, Zulfikar R, Stansbury R. Coal mining and lung disease in the 21st century. *Curr Opin Pulm Med.* 2020;26(2):135–41.
27. Go L, Cohen RA. Coal workers' pneumoconiosis and other mining-related lung disease. *Clin Chest Med.* 2020;41(4):687–96.

28. Yu P, Zhao J, Hao X, Sun X, Ling M. Computer aided detection for pneumoconiosis based on co-occurrence matrices analysis. In: International Conference on Biomedical Engineering & Informatics: 2009; 2009.
29. Sundararajan R, Xu H, Annangi P, Tao X, Mao L. A multiresolution support vector machine based algorithm for pneumoconiosis detection from chest radiographs. In: Proceedings of the 2010 IEEE International Symposium on Biomedical Imaging: From Nano to Macro, Rotterdam, The Netherlands, 14–17 April, 2010.
30. Agrawal T, Choudhary P. Segmentation and classification on chest radiography: a systematic survey. *Vis Comput.* 2023;39(3):875–913.
31. Shorten C, Khoshgoftaar TM. A survey on image data augmentation for deep learning. *J Big Data.* 2019; 6(1).
32. Lumini A: Comparison of different image data augmentation approaches. *J Imag.* 2021; 7.
33. Chlap P, Min H, Vandenberg N, Dowling J, Holloway L, Haworth A. A review of medical image data augmentation techniques for deep learning applications. *J Med Imaging Radiat Oncol.* 2021;65(5):545–63.
34. Gu J, Wang Z, Kuen J, Ma L, Shahroudy A. Recent advances in convolutional neural networks. *Pattern Recogn J Pattern Recogn Soc.* 2018;77:354.
35. Huang G, Liu Z, Laurens V, Weinberger KQ. Densely connected convolutional networks. *IEEE Computer Society* 2016.
36. Liu Z, Zhu Y, Yuan Y, Yang L, Wang K, Wang M, Yang X, Wu X, Tian X, Zhang R et al. 3D DenseNet deep learning based preoperative computed tomography for detecting myasthenia gravis in patients with thymoma. *Front Oncol.* 2021; 11.
37. Wang Q, Wu B, Zhu P, Li P, Hu Q: ECA-Net: efficient channel attention for deep convolutional neural networks. In: 2020 IEEE/CVF Conference on Computer Vision and Pattern Recognition (CVPR): 2020; 2020.
38. Qi A, Tian N. Fine-grained vehicle recognition method based on improved ResNet. In: 2020 2nd International Conference on Information Technology and Computer Application (ITCA): 2020; 2020.
39. Zhang Y, Weng Y, Lund J. Applications of explainable artificial intelligence in diagnosis and surgery. *Diagnostics.* 2022;12(2):237.

Publisher's Note

Springer Nature remains neutral with regard to jurisdictional claims in published maps and institutional affiliations.